Toward the Next-Generation Nanomedicines: Design of Multifunctional Multiblock Polyurethanes for Effective Cancer Treatment

Mingming Ding,[†] Nijia Song,[†] Xueling He,[‡] Jiehua Li,[†] Lijuan Zhou,[†] Hong Tan,[†,*] Qiang Fu,[†] and Qun Gu[§]

[†]College of Polymer Science and Engineering, State Key Laboratory of Polymer Materials Engineering, Sichuan University, Chengdu 610065, China, [‡]Laboratory Animal Center of Sichuan University, Chengdu 610041, China, and [§]Ningbo Key Laboratory of Polymer Materials, Ningbo Institute of Material Technology and Engineering, Chinese Academy of Sciences, Ningbo 315201, China

ABSTRACT Specific accumulation of therapeutics at tumor sites to improve *in vivo* biodistribution and therapeutic efficacy of anticancer drugs is a major challenge for cancer therapy. Herein, we demonstrate a new generation of intelligent nanosystem integrating multiple functionalities in a single carrier based on multifunctional multiblock polyurethane (MMPU). The smart nanocarriers equipped with stealth, active targeting, and internalizable properties can ferry paclitaxel selectively into tumor tissue, rapidly enter cancer cells, and controllably release their payload in response to an intracellular acidic environment, thus resulting in an improved biodistribution and excellent antitumor activity *in vivo*. Our work provides a facile and versatile approach for the design and fabrication of smart intracellular targeted nanovehicles for effective cancer treatment, and opens a new era in the development of biodegradable polyurethanes for next-generation nanodelivery systems.

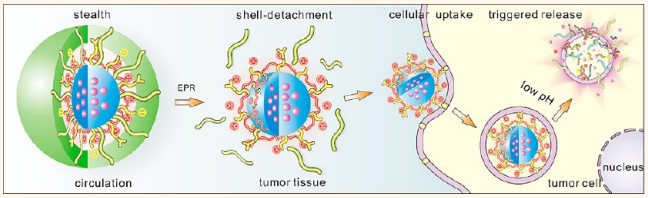

KEYWORDS: intelligent · biodegradable multifunctional multiblock polyurethane · stimuli-responsive · nanomedicine · intracellular drug delivery · target · cancer therapy

A major bottleneck in cancer therapy is to achieve specific drug accumulation at tumor sites, because most chemotherapeutic agents are unable to differentiate between diseased and healthy cells, leading to poor biodistribution and undesired side effects. This obstacle can be potentially overcome by a targeted delivery approach using multifunctional nanodelivery systems.[1−3] To date, there are several nanotechnology-based therapeutic products clinically approved by the Food and Drug Administration (FDA) for cancer treatment, and more are undergoing clinical trials.[4,5] However, the clinical translation of targeted/multifunctional drug delivery is not as smooth as expected, which is evidenced by the fact that all the approved nanoformulations, including liposomal doxorubicin, paclitaxel-loaded poly(ethylene glycol)-poly(L-lactide) micelles, and albumin-based nanoparticles, *etc.*, appear relatively simple and universally lack active targeting, triggered release, or other functional components.[5−7] This is mainly because current multifunctional nanomedicines developed for cancer therapy suffer from serious limitations. A principal challenge is how to establish the optimal interplay of factors that confer long circulation, tumor targeting, cell internalization, and controlled release to overcome the physiological barriers *in vivo*.[8] Given that all the parameters are interactional and improving one may often negatively impact another, the nanocarriers are required to coordinate these functionalities intelligently and make them work in concert.[9,10] Another barrier arises from the difficulty and complexity behind manufacturing viable targeted multifunctional nanovehicles.[11−13] Since normal diblock or triblock copolymers lack reactive sites for modification or functionalization, considerable attention has been focused on the use of complex molecules (*e.g.*, dendritic, hyperbranched, and star-shaped copolymers, *etc.*), which could provide more control and lead to a number of possibilities for fabricating novel nanostructures

* Address correspondence to hongtan@scu.edu.cn.

Received for review April 7, 2012 and accepted February 14, 2013.

Published online February 14, 2013
10.1021/nn4002769

© 2013 American Chemical Society

and nanomaterials with multiple functionalities.[14−20] Unfortunately, many of these materials are nonbiodegradable or nonbiocompatible, and most of them require a rather complicated synthesis and purification process.[14,21,22] Alternatively, recent emerging modular "mix-and-match" methodology offers a new opportunity to combine multiple components with different properties into a nanosystem,[23−25] while it still faces tremendous unknown difficulties, such as structural uncertainty in individual and mixed micellar systems, batch-to-batch variation, and insufficient stability *in vivo*.[26−28] Therefore, there is an urgent need for a new generation of formulations meeting all required attributes in a simple and scalable nanocarrier platform that can provide safe and effective delivery of various pharmaceutical agents.

Polyurethane may be a promising choice for addressing this need. Since introduced as implantable biomaterials in 1967,[29] polyurethanes have been well established as one of the most versatile materials used for a broad range of biomedical applications, and some have been commercially applied in clinic as heart valves, catheters, and wound dressings.[30] The facile preparation and highly variable chemistry of polyurethanes may enable the incorporation of different functional moieties, such as stimuli responsiveness, targeting molecules and internalizable ligands, into the polymer structure to generate biodegradable and biocompatible nanoassemblies exhibiting diverse physicochemical properties, which would be appealing candidates in the clinical exploration of next generation nanotherapeutics for smart drug delivery.[31] However, the development of nanoformulations that satisfy these criteria has so far been seldom reported.

Herein, we design an intelligent all-in-one nanosystem integrating various desired functions in a single carrier *via* a facile multiblock strategy, by virtue of the good biocompatibility, unique architecture, and excellent molecular tailorability provided by multifunctional multiblock polyurethane (MMPU) (Figure 1A). The soft segments of MMPU are based on hydrophobic biodegradable poly(ε-caprolactone) bearing pH-responsive hydrazone bonds (HPCL) for the accommodation of lipophilic agents in physiological conditions and triggered release of drugs in response to an intracellular acidic environment. The hard segments were constructed from nontoxic L-lysine ethyl ester diisocyanate (LDI) and 1,3-propanediol (PDO) for the formation of polyurethanes with satisfactory molecular weight and relatively good biocompatibility. The side chains comprise both cell penetrating gemini quaternary ammonium (GQA) cationic groups and tripeptide containing reactive carboxyl anion groups that can enhance the cell internalization of nanocarriers and provide an active site for further conjugation of targeting antibodies, respectively.[32] To achieve the stealthlike character of nanovehicles, the polymer chain ends were terminated by the attachment of hydrophilic methoxyl-poly(ethylene glycol) with an acidic-cleavable hydrazone linkage (HPEG), which was expected to provide good protection for carriers and ligands in circulation, and to be detached under acidic tumor environment for maximizing the targeting effect and intracellular delivery of antitumor drugs.

RESULTS AND DISCUSSION

To obtain these multiblock polyurethanes, a series of functional monomers were synthesized according to our previous reports,[33−38] and the copolymers were prepared *via* a facile three-step polymerization as illustrated in Figure S1 (see Supporting Information for details). The resultant polymers present well-controlled architectures and moderate molecular weights (M_n is about 12500−29800) with monodisperse and quite narrow molecular weight distributions (Table 1 and Supporting Information, Figure S2). The content of hydrazone bonds and gemini cationic groups in copolymers can be easily tuned by the feed ratios (Supporting Information, Table S1).

The prepared MMPUs could self-assemble into nanomicelles in an aqueous solution, where an insoluble HPCL segment constitutes a hydrophobic core, surrounded by outer shells formed by hydrophilic blocks including GQA, tripeptide and HPEG. The multiblock architecture of MMPU and the core−shell−corona structure of micelles were first characterized with nuclear magnetic resonance (NMR) spectroscopy. As depicted in Figure 1B, the characteristics of HPCL, LDI, HPEG, and GQA segments are well detected in deuterated dimethyl sulfoxide (DMSO-d_6) (see also Supporting Information, Figure S3). By contrast, the resonances of HPCL and GQA are significantly weakened and that of HPEG (3.71 ppm) is clearly enhanced in D_2O (Figure 1B). This is strongly indicative of the self-assembly of MMPU into a core−shell−corona system. The formation of the micellar structure was also confirmed by fluorescence measurement (Supporting Information, Figure S4). To visually demonstrate the unique architecture of the MMPU micelles, computational simulation was performed using a dissipative particle dynamics (DPD) method (Supporting Information). As seen from the cross-section view and density profile of nanocarriers (Figure 1C and Supporting Information, Figure S5), a multilayered micellar structure comprising PCL core, gemini, and tripeptide shells as well as PEG corona are well-defined, which is in good agreement with ^{1}H NMR results. These nanocarriers appear as dispersed individual particles with irregular spherical, cylindrical, or worm-like shapes and diameters in the range of 51.8−98.5 nm, as determined by transmission electron microscopy (TEM) observation and size measurements (Figure 1C,D, Table 1). Furthermore, they display low critical micelle concentrations (CMCs, 1.1−3.3 $\times$ 10^{-3}

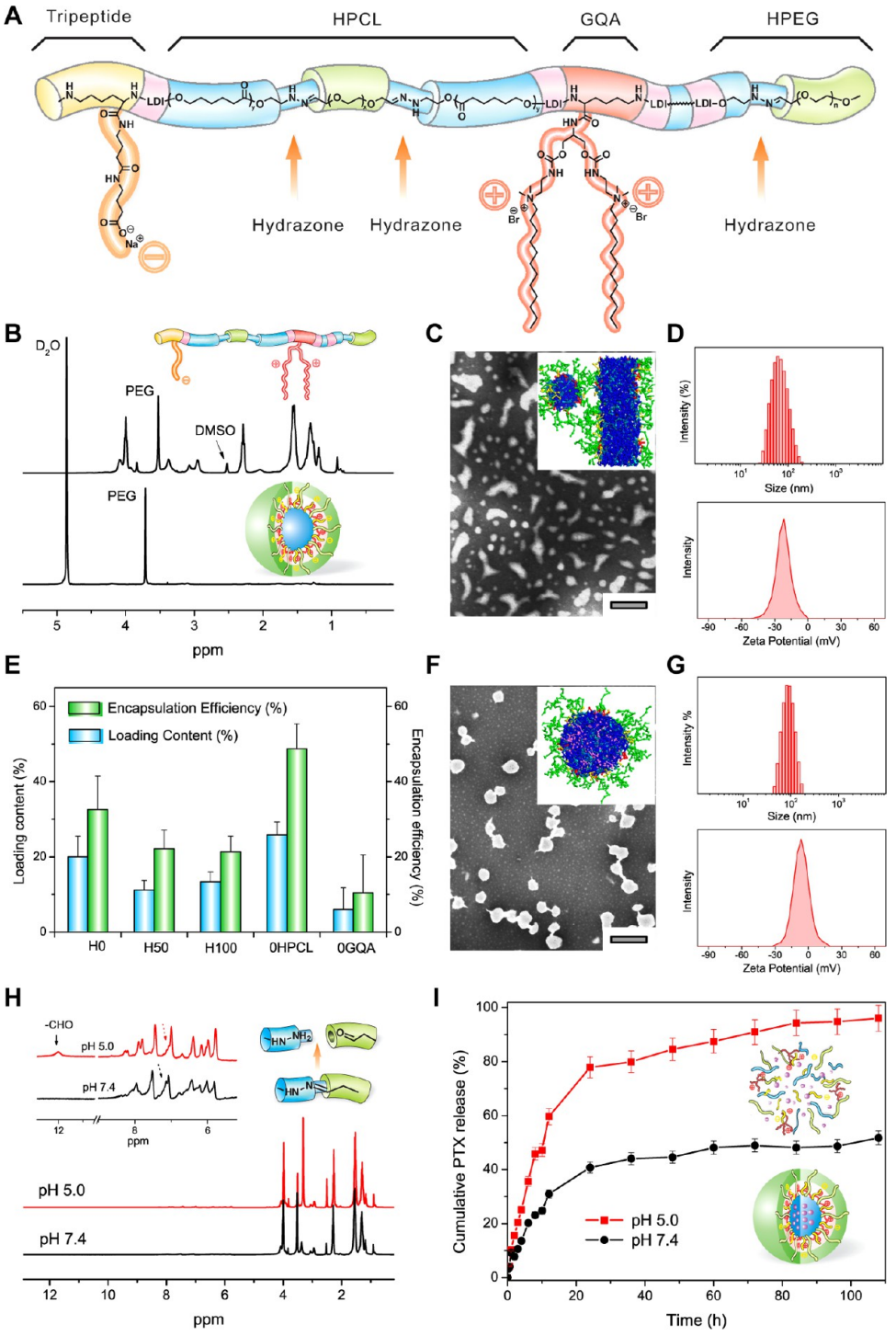

Figure 1. (A) Schematic molecular structure of multifunctional multiblock polyurethane. (B) ^{1}H NMR spectra of MMPU (H100) in DMSO-d_6 (30 mg/mL) and its micelles in D_2O (1 mg/mL). The insets show schematic structures of MMPU and the self-assembled nanomicelle. (C−G) TEM images (C,F) and size and zeta potential (D,G) of MMPU micelles (C,D) and PTX-loaded micelles (F,G) prepared from H100. Scale bars, 200 nm. The insets in panels C and F show cross-sectional views of micellar structures of blank and PTX-loaded MMPU micelles from DPD simulations, respectively. Color code: blue, PCL; red, GQA; yellow, tripeptide; green, PEG; magenta, PTX. (E) Drug loading content and encapsulation efficiency for PTX loaded in MMPU nanomicelles. (H) ^{1}H NMR spectra of MMPU nanocarrier after degradation for 24 h at pH 5.0 and 7.4. (I) Time-dependent cumulative release of PTX from MMPU micelles at different pH values.

mg/mL) (Table 1 and Supporting Information, Figure S4) and high drug loading capacity for the anticancer drug paclitaxel (PTX) (drug loading content up to 26%, Figure 1E and Supporting Information, Figure S6). The drug-encapsulated nanocarriers also exhibit irregular shapes with no appreciable change of particle size and zeta potential in comparison with blank micelles (Figure 1F and G), implying a good stability of the

TABLE 1. Characteristics of Multifunctional Multiblock Polyurethanes and Their Micelles

samples[a]	M_n (g/mol)[b]	M_w (g/mol)[b]	M_w/M_n[b]	size (nm)[c]	PDI[c]	zeta potential (mV)[c]	CMC (10^{-3} mg/mL)[d]
H0	29800	33300	1.12	51.8 ± 3.3	0.215	−18.0 ± 1.4	1.22
H20	12500	13700	1.09	87.4 ± 1.8	0.045	−15.6 ± 0.1	1.31
H50	28200	47000	1.66	98.5 ± 1.4	0.076	−30.5 ± 0.3	3.32
H80	22200	26200	1.18	67.3 ± 0.8	0.021	−35.0 ± 2.3	1.37
H100	27200	43500	1.60	61.7 ± 4.2	0.293	−21.7 ± 0.5	1.11
0HPCL	12500	16400	1.32	88.4 ± 3.8	0.038	−33.9 ± 0.6	2.98
0GQA	22000	26100	1.18	86.0 ± 3.4	0.156	−61.3 ± 1.2	1.34

[a] Multifunctional multiblock polyurethanes are denoted as H*X*, where *X* is the molar content of HPEG in end-capping reagents. 0HPCL and 0GQA represent MMPUs without HPCL and GQA, respectively. [b] Molecular weights and molecular weight distributions of MMPUs were determined by GPC. [c] Sizes, size distributions (PDI), and zeta potentials were measured with a Zetasizer Nano ZS dynamic light scattering (DLS) instrument (Malvern, UK). [d] Critical micelle concentration (CMC) was determined by a fluorescence probe method using pyrene as a hydrophobic probe.

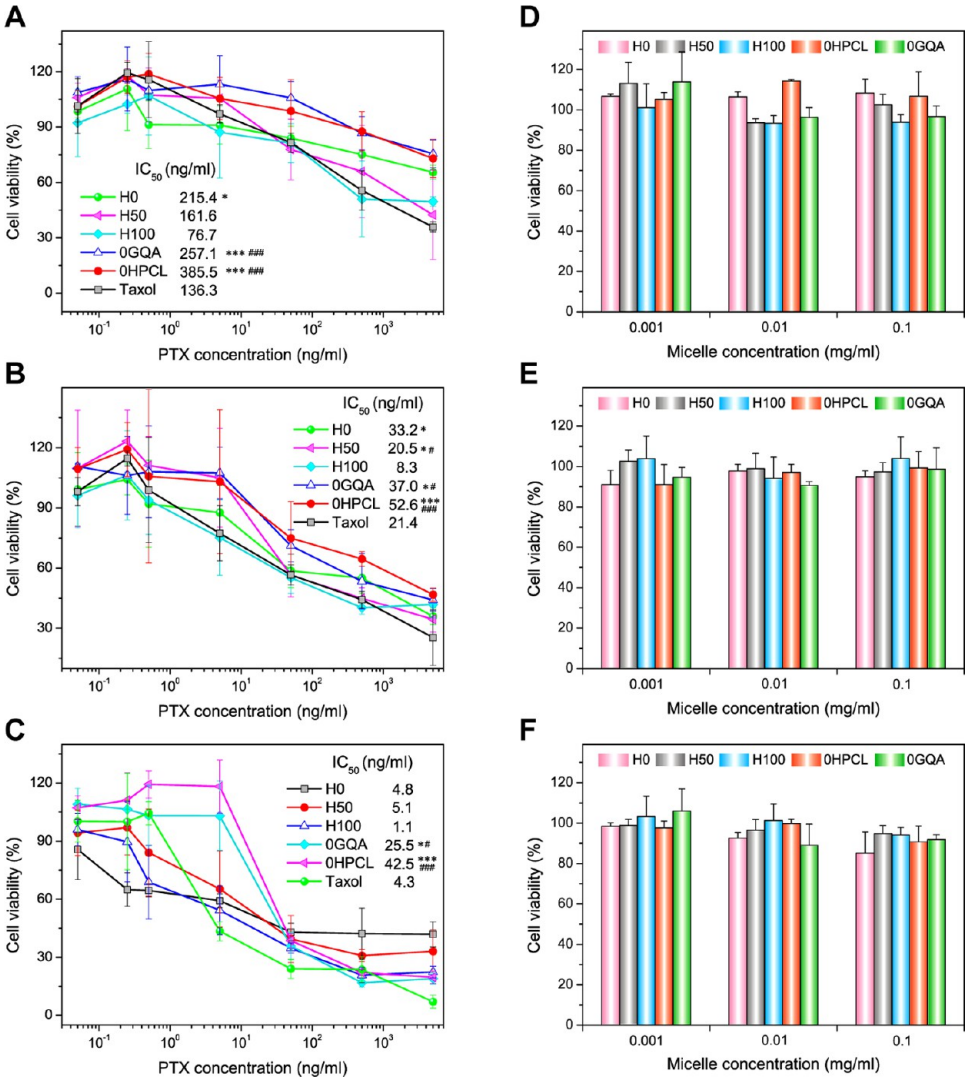

Figure 2. Drug efficacy of PTX-loaded MMPU nanomicelles against A431 tumor cells (A−C) and cytotoxicity of blank MMPU nanomicelles toward 3T3 mouse fibroblasts (D−F) after 24 h (A,D), 48 h (B,E), and 72 h (C,F) of incubation. Statistical significance: (∗) $P < 0.05$; (∗∗) $P < 0.01$; (∗∗∗) $P < 0.005$ vs H100; (#) $P < 0.05$; (##) $P < 0.01$; (###) $P < 0.005$ vs Taxol.

nanosystems. This was further verified by the DPD simulation result, where PTX molecules are well-distributed in the PCL inner core (Figure 1F and Supporting Information, Figure S5). In addition, all micelle formulations show negative surface charges ranging from −61.3 to −15.6 mV under neutral conditions (Table 1), which favors protein resistance and prolonged circulation time for *in vivo* applications. Interestingly, at lower pH values, the micelles become positively charged, and the sizes grow slightly due to

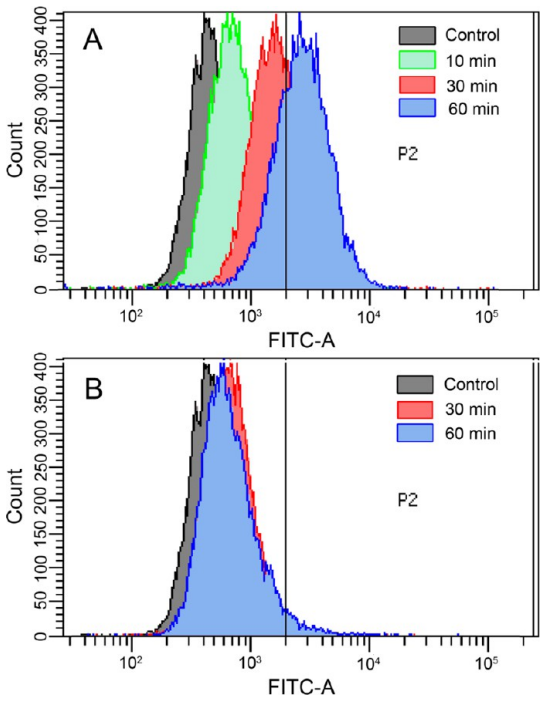

Figure 3. Flow cytometry histogram profiles of A431 cells incubated with C225-conjugated MMPU nanocarriers (A) and nontargeted nanocarriers (B) for different times.

the deionization of carboxyl groups and partial detachment of the HPEG shell resulting in an exposure of cationic GQA groups (Supporting Information, Figure S7). This phenomenon is helpful to cell internalization and subsequent endosomal escape of polyurethane nanocarriers within tumor cells.[39,40] It is noticed that the hydrazone linkages attached to the PEG chains at carrier surfaces appear preferentially subjected to acidolysis, rendering a detachment of the outer corona before micelle disintegration. With longer incubation at pH ≈ 5.0, the hydrazone bonds embedded in the core-forming HPCL block are cleaved and the micelles get disassembled (Figure 1H, Supporting Information, Figures S7, S8). Meanwhile, the molecular weights of polymers are significantly decreased, and the extent of degradation increases with increasing content of hydrazone linkages in the polyurethane backbone (Supporting Information, Figure S9 and Table S2). As a result, a largely accelerated release of PTX was observed in weak acid solutions (pH ≈ 5.0, Figure 1I). Considering that the drug carriers may be trapped in acidic endosomes (pH 5−6) or lysosomes (pH 4−5) within tumor cells after receptor-mediated endocytosis,[41] a triggered intracellular release and subsequently an increased cytotoxicity can be anticipated

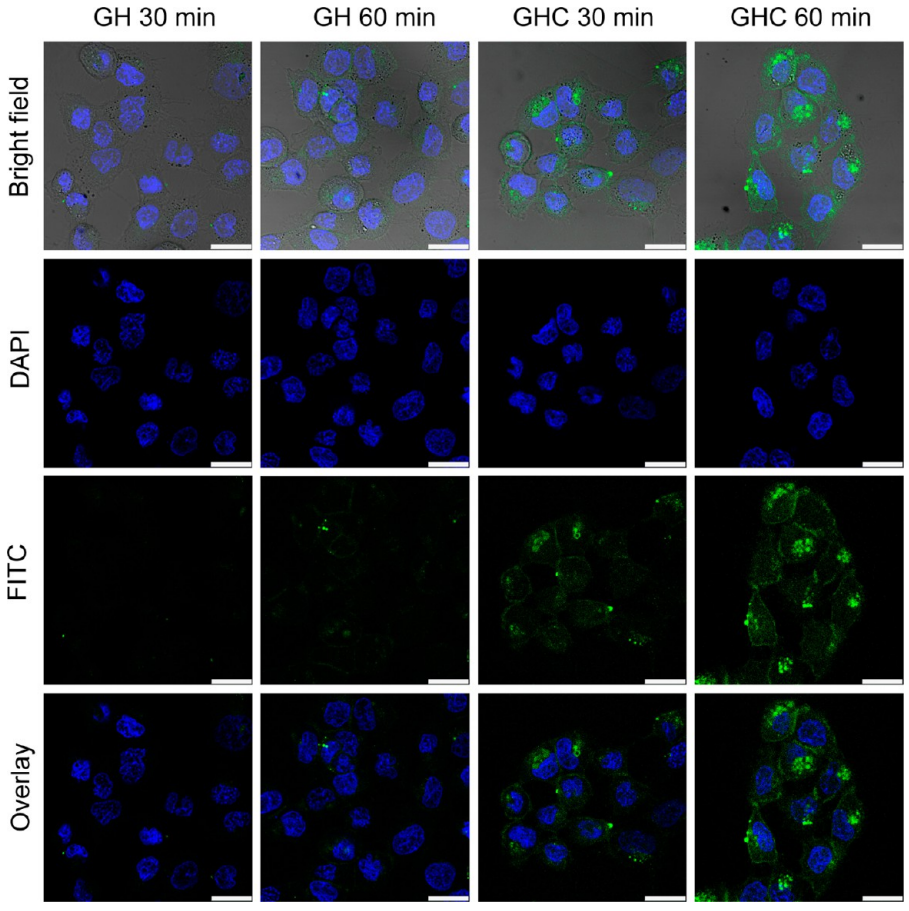

Figure 4. CLSM images of A431 cells incubated with C225-conjugated MMPU nanocarriers (GHC) and nontargeted nanocarriers (GH) for different times. Scale bars, 25 μm. MMPU nanocarriers were labeled with fluorescein isothiocyanate isomer I (FITC, green), nuclei of cells were stained with 2-(4-amidinophenyl)-6-indolecarbamidine dihydrochloride (DAPI, blue).

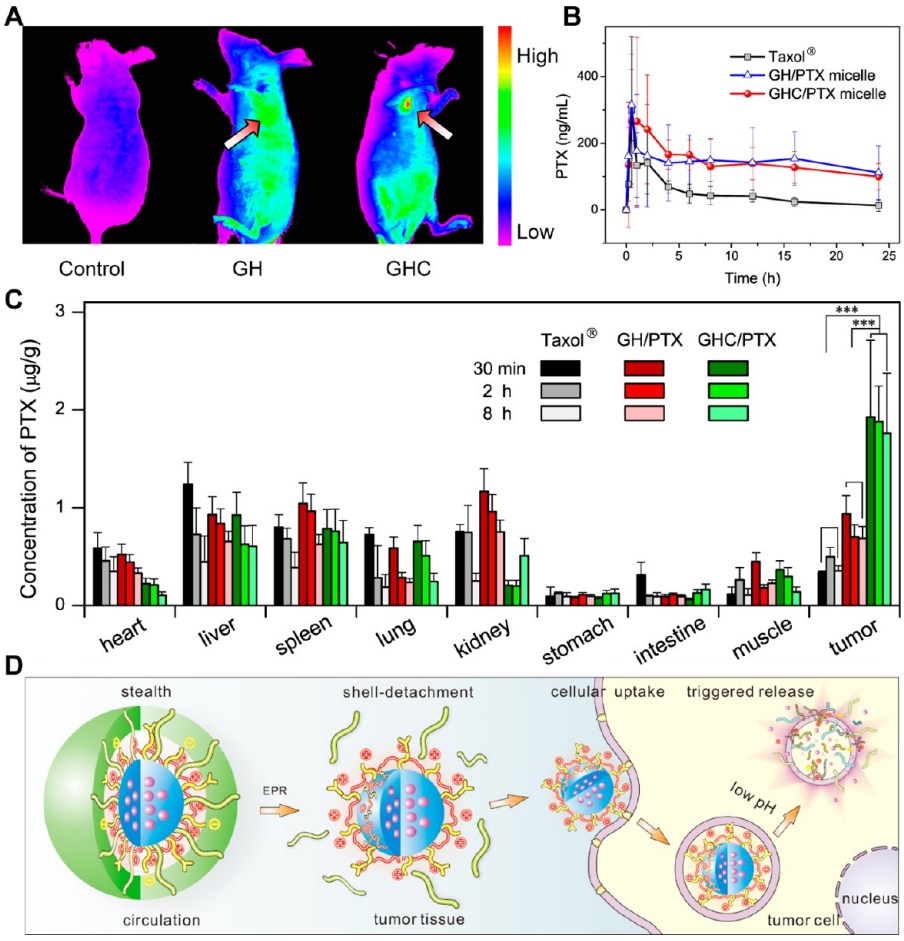

Figure 5. (A) *In vivo* fluorescence images of control mice and tumor-bearing nude mice receiving intravenous injection of fluorescent-labeled MMPU nanomicelles after 60 min. Arrows show A431 tumor in mice. (B) Plasma concentration−time profiles of PTX after intravenous injection of Taxol, GH/PTX, and GHC/PTX formulations at 5.0 mg/kg dose in rats. Error bars represent means ± standard deviation for $n = 6$. (C) Tissue distribution profiles of PTX after intravenous administration of Taxol and micellar formulations at a dose of 5 mg/kg in nude mice. Statistical significance: (*) $P < 0.05$; (**) $P < 0.01$; (***) $P < 0.005$. (D) Schematic mechanism of targeted intracellular delivery of anticancer drugs into tumor cells using MMPU nanocarriers.

for these nanomedicines. To demonstrate this potential, the *in vitro* anticancer activity of MMPU formulations was evaluated on human A431 squamous carcinoma tumor cells and compared with commercial Taxol. As expected, the PTX-loaded multifunctional H100 micelles show very high drug efficacy against cancer cells *in vitro*, with median inhibitory concentrations (IC_{50}) (76.7, 8.3, and 1.1 ng/mL) much lower than those of other formulations without an acidic-degradable core (0HPCL, 385.5, 52.6, and 42.5 ng/mL) or cell-internalizable gemini shell (0GQA, 257.1, 37.0, and 25.5 ng/mL), and comparable to those of Taxol (136.3, 21.4, and 4.3 ng/mL) after incubation for 24, 48, and 72 h, respectively (Figure 2A−C). Furthermore, the blank micelles do not show any toxic effect toward 3T3 mouse fibroblasts at a high concentration up to 0.1 mg/mL (Figure 2D−F), indicating that MMPU itself is not responsible for the cytotoxicty, and these micelles are potentially safe to be used as pharmaceutical nanovehicles.

To endow multifunctional nanocarriers with improved specificity and selectivity, taking H100 as an example, an antiepidermal growth factor receptor (EGFR) monoclonal antibody cetuximab (C225) was chemically attached onto the micellar surface through the carboxyl groups of tripeptide (see Supporting Information). C225 is a chimeric immunoglobulin G1 monoclonal antibody that targets the extracellular domain of EGFR overexpressed in a wide variety of cancers.[42] The success of antibody conjugation was verified *via* both an enzyme-linked immunosorbent assay (ELISA) and NMR measurement, and the purity of immunomicelles was confirmed with size exclusion chromatogram (SEC) (Supporting Information, Figure S10). After conjugation of C225, the nanomicelles display some irregular spherical and cylindrical shapes, with slightly increased size and zeta potential over unconjugated nanocarriers (Supporting Information, Figure S10). To study the specific binding and uptake of targeted-MMPU nanocarriers by EGFR-overexpressing A431 tumor cells, flow cytometry, fluorescence microscopy, and confocal laser scanning microscopy (CLSM) were performed. It was found that nontargeted

micelles (GH) show little internalization, with a faint signal observed in tumor cells. In contrast, the cellular uptake of C225-conjugated nanocarriers (GHC) is almost 18-fold greater than that of GH after 60 min of incubation and the strong fluorescence is localized predominantly in the cytoplasm (Figures 3 and 4 and Supporting Information, Figure S11), suggesting that the cell entry of targeted GHC is probably based on a ligand-mediated mechanism resulting in a greater amount of micelles internalized inside tumor cells.[43,44] In addition, normal 3T3 mouse fibroblasts used as EGFR-negative controls show little fluorescence for all the formulations (Supporting Information, Figures S11,S12). These results directly demonstrate that the cellular targeting of MMPU nanomicelles can be enhanced by covalent binding of C225 onto their surfaces and the targeting effect is highly selective for EGFR-enriched tumor cells.

To investigate whether the incorporation of multiple functionalities into MMPU nanocarriers enables improved biodistribution *in vivo*, GHC and GH micelles were labeled with FITC and intravenously administered into the tail vein of mice bearing the A431 tumor model. The mice receiving targeted GHC micelles display a strong FITC fluorescence at the tumor site at 60 min after injection, while those receiving nontargeted GH formulations exhibit much weaker fluorescence intensity in the tumor region (Figure 5A). To better understand the mechanism of such rapid tumor accumulation, we examined the pharmacokinetics and tissue distributions of multifunctional polyurethane nanomicelles. The plasma concentration–time profiles of PTX for various formulations are presented in Figure 5B. In comparison with commercial Taxol, both micellar formulations significantly increase the retention time of PTX in the blood. Furthermore, GHC/PTX shows much greater drug accumulation in tumor tissue than nontargeted GH/PTX and Taxol ($P < 0.005$, Figure 5C). In particular, the concentration ratios of PTX in tumor to those in liver and spleen are 2.1 and 2.5, respectively, for GHC/PTX immunomicelles, compared with those of 1.0 and 0.9, respectively, for GH/PTX formulations at 30 min postinjection (Figure 5C). It has been shown that an enhanced plasma half-life would not necessarily result in an increase in tumor accumulation of therapeutics due to limited penetration of drugs into tumors.[45,46] Therefore, other than enhanced permeability and retention (EPR) effect, the active targeting and specific intracellular delivery of drug formulations may be the key contributions to the satisfactory tissue distribution achieved in this study (Figure 5D).

To evaluate whether the efficient targeting and improved biodistribution can lead to enhanced therapeutic efficacy, GH/PTX, GHC/PTX, Taxol, and phosphate buffered saline (PBS, pH 7.4) as controls were injected into A431 tumor-bearing nude mice *via* the tail vein. No mice died during the treatment period (Supporting Information, Figure S13). Compared with the control group, Taxol and PTX-loaded MMPU micelles exhibit a considerable tumor inhibition *in vivo*, and the micellar formulations possess much higher antitumor activity than Taxol even at relatively lower dose ($P < 0.05$, Figure 6), regardless of their comparable cytotoxicity to Taxol toward tumor cells *in vitro* (Figure 2). This is because Taxol lacks protective vehicle and targeting specificity, and thus is quickly cleared from the bloodstream (Figure 5B) and results in a much lower PTX concentration in tumor tissue than those for micellar formulations (Figure 5C). In addition, the

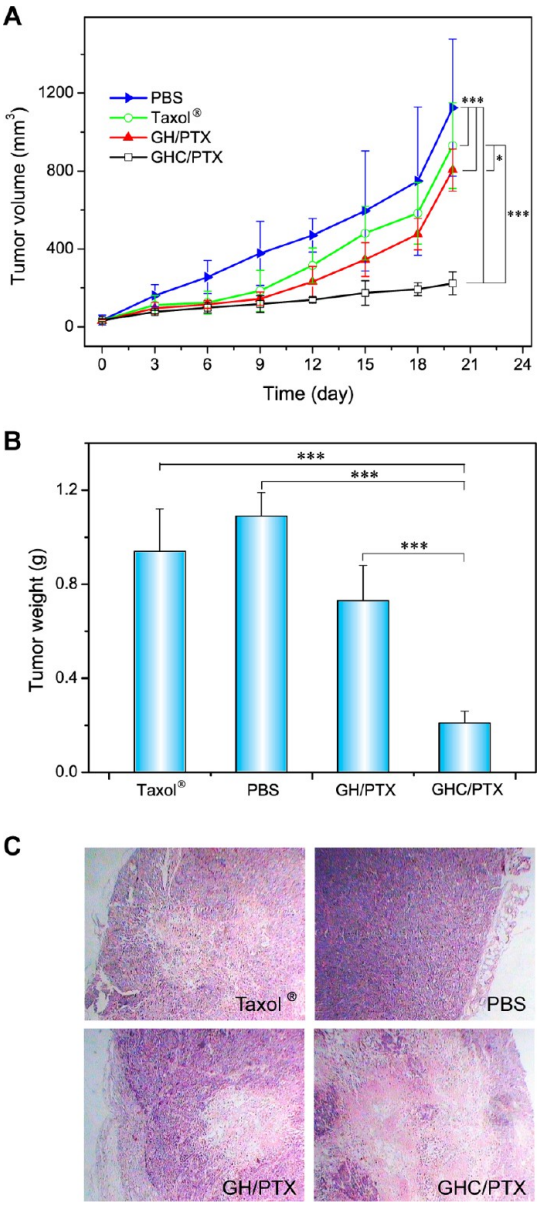

Figure 6. (A) Changes of tumor volume after intravenous injection of PBS, Taxol, GH/PTX, and GHC/PTX formulations in A431 tumor-bearing nude mice. (B,C) Mean weights (B) and sections (C) of tumors separated from animals receiving different treatments. Statistical significance: (*) $P < 0.05$; (**) $P < 0.01$; (***) $P < 0.005$.

volume of tumor treated with targeted GHC/PTX is 3-fold and 4-fold smaller than those treated with nontargeted GH/PTX and Taxol at the end of 20 d, respectively (Figure 6A and Supporting Information, Figure S13). The tumor weight inhibition (TWI) obtained from the weights of excised tumors is 80.3% for targeted GHC/PTX (Figure 6B), which is significantly higher than those for the nontargeted system and Taxol, and even higher than those reported for other PTX nanoformulations.[47,48] Furthermore, GHC/PTX manifests the highest efficiency concerning the prevention of cancer cell expansion as evidenced from the histological analysis of tumor sections (Figure 6C). As additional controls, empty micelles (GH and GHC) without drug incorporation were also tested and did not produce any measurable inhibition effect on tumor growth (Supporting Information, Figure S14). These results reveal that the superior therapeutic efficacy of the GHC/PTX formulation is attributed to the higher amount of PTX that reached the tumor site *via* multifunctional targeted delivery and not to the drug action mediated by C225 itself or other polymer components.[49,50] This is expected since the dose of C225 antibody used for targeting herein is much lower than that required for therapy.[43,51] Overall, our work demonstrates that biodegradable MMPU can act as an ideal nanoplatform for smart targeted delivery of chemotherapeutic drugs into tumors for high-effective cancer treatment. To evaluate the *in vivo* toxic effect of multifunctional nanoformulations, maximum tolerance dose studies are needed and being carried out in our group.

CONCLUSION

We have designed and prepared an intelligent nanosystem based on multifunctional multiblock polyurethanes for targeted intracellular delivery of PTX into tumors. These nanocarriers demonstrate a variety of attractive properties in a smart fashion, such as stealth character and long circulation, active targeting, pH-dependent shell-detachment on arriving at tumor site, improved cellular internalization, and triggered intracellular drug release in response to acidity within tumor cells. As a result, they can greatly improve the biodistribution and anticancer efficacy of chemotherapeutic drugs *in vivo*. This study provides a facile and versatile approach for the design and construction of multifunctional intracellular targeted nanovehicles for effective cancer treatment and opens a new era in the development of multiblock polyurethanes in smart drug delivery applications. Future studies combining other drugs, genetic materials, or imaging agents will assess the applicability of theranostic nanoplatforms for realizing personalized gene therapy and chemotherapy. In addition, the further optimization of synthesis chemistry and technology to develop MMPUs with better-defined and well-controlled architectures is of great significance for producing desired nanomedicine products and, more importantly, for making them easy to be approved by FDA and translated into the clinic.

MATERIALS AND METHODS

Materials. A series of functional monomers including L-lysine-derivatized GQA, L-lysine-γ-aminobutyric acid-γ-aminobutyric acid tripeptide, HPCL, and HPEG were synthesized in our laboratory according to previous reports.[33−38] Antiepidermal growth factor receptor monoclonal antibody cetuximab (C225) was purchased from Harbin Pharmaceutical Group Co., Ltd., China. Paclitaxel (PTX, 99.5%) was obtained from Shanghai Jinhe Bio-Technology Co., Ltd., China. Taxol was commercially available from West China Hospital, Sichuan University, China. 3-(4,5-Dimethylthiazol-2-yl)-2,5-diphenyl tetrazolium bromide (MTT) and Nile red (NR, 98.0%) were purchased from Sigma-Aldrich, USA. 2-(4-Amidinophenyl)-6-indolecarbamidine dihydrochloride (DAPI) was obtained from Roche Diagnostics, Germany. Fluorescein isothiocyanate isomer I (FITC, 90%) was from Acros Organics, USA. Methyl *tert*-butyl ether (MTBE, chromatographic grade) was purchased from Shanghai Jingchun Chemical Co., Ltd., China.

Synthesis of MMPU. Multifunctional multiblock polyurethane (MMPU) was synthesized *via* a facile three-step polymerization as described in the Supporting Information.

Preparation of MMPU Nanocarriers. The self-assembled polyurethane nanomicelles were prepared with a dialysis method. Coupling of C225 to the nanocarriers was performed by utilizing the carboxyl groups of tripeptide on the particle surface. Details for the preparation and characterization of MMPU nanocarriers were provided in the Supporting Information.

Stimuli-Responsiveness. HCl and NaOH were used to adjust the micellar solutions to pH $\approx$ 5.0−7.4. The pH- and time-dependent variation of size and surface charge of MMPU micelles were recorded. The degradation products obtained by 24 h of incubation at pH $\approx$ 5 were lyophilized for ^{1}H NMR and gel permeation chromatography (GPC) analysis (Supporting Information).

Drug Loading and Controlled Release. PTX was loaded into MMPU nanocarriers with a micelle extraction technique.[32] Briefly, a drug stock solution in acetone was added to an empty vial. After evaporation of the solvent, 10 mL of micellar solution was transferred into the vial and ultrasonated for 2 h. The solution was centrifugalized at 3000 r/min for 10 min and passed through a 0.45 μm pore-sized syringe filter (Millipore, Carrigtwohill, Co. Cork, Ireland).

The release of PTX was conducted using a dialysis method in phosphate buffer solution (PBS, 10 mM, pH 7.4) and acetate buffer solution (ABS, 10 mM, pH 5.0) at 37 °C with shaking. The release media also contains 100 mM sodium salicylate to maintain a sink condition.[52] At desired time intervals, 3 mL of release media was sampled and replenished with an equal volume of fresh media. The release experiments were conducted in triplicate.

The PTX concentration was determined by a model LC-6A high-performance liquid chromatography (HPLC) system (Shimadzu, Kyoto, Japan) equipped with a reverse-phase C18 column (4.6 $\times$ 250 mm, 5 μm) and an SPD-6AV detector. The flow rate was 1.0 mL/min, and the mobile phase consisted of acetonitrile/water (60/40 v/v). The detection of PTX was performed by UV absorption at 227 nm.

Cell Viability Assay. To test the cytotoxicity of MMPU nanomicelles toward normal cells and the drug efficacy of PTX-loaded MMPU micelles against cancer cells, 3T3 mouse fibroblasts and A431 cells were seeded in 96-well plates and incubated for 24 h.

The 3T3 cells were treated with 100 μL of medium containing various concentrations of drug-free micelle solutions for 24, 48, and 72 h, and the A431 cells were exposed to drug-loaded micelles containing different amounts of PTX at 37 °C for 24, 48, and 72 h. Then 20 μL of MTT solution was added to each well. After incubating the cells for 4 h, the MTT solution was removed and the insoluble formazan crystals were dissolved in 100 μL of DMSO. The absorbance was measured at a wavelength of 490 nm. The cell viability was evaluated and normalized using untreated cells as a control. The dose−effect curves were made and IC_{50} values were calculated using the software GraphPad Prism 5 for Windows (GraphPad Software, Inc., San Diego, CA) according to the following equation: Y = Bottom + (Top − Bottom)/(1 + $10^{((\mathrm{Log}\ IC_{50} - X) \times \mathrm{HillSlope})}$), where X is the logarithm of drug concentration, and Y is the response. Top and Bottom are the Y-values at the top plateau and bottom plateau, respectively, and HillSlope describes the steepness of the family of curves.

Cellular Uptake. For flow cytometry, EGFR-overexpressing A431 tumor cells and EGFR-negative 3T3 mouse fibroblasts[53] were seeded into 6-well culture plates and grown for 24 h. The cells were then treated with FITC-labeled MMPU nanomicelles at 37 °C for 10, 30, and 60 min. Thereafter, culture medium was removed and cells were washed with PBS three times and treated with trypsin. After removing the supernate, the cells were resuspended in 0.5 mL PBS, and analyzed using an FACS Aria flow cytometer (BD biosciences) by counting 10 000 events.

For CLSM, A431 cells were seeded at a density of 1×10^5 cells/well in 6-well chamber slides for 24 h. The cells were incubated with FITC-encapsulated micelle for 30 and 60 min at 37 °C. After removal of the medium, the cells were washed three times with cold PBS, fixed with 1 mL of 4% paraformaldehyde in PBS for 30 min at 4 °C, and stained with DAPI for 10 min. Finally, the slides were mounted with 10% glycerol solution and observed using a TCS SP 5 confocal laser scanning microscope (CLSM, Leica, Germany). To provide more evidence of cellular targeting and uptake, Nile red as a fluorescent dye was also used to label the MMPU nanocarriers for fluorescence microscope observations (Supporting Information).

Animals and Tumor Models. The animal studies were carried out with the approval from the Ethics Committee of Sichuan University and in compliance with the Principles of Laboratory Animal Care of the National Institutes of Health, China. Adult Sprague−Dawley (SD) rats (200 ± 20 g) and 6-week-old athymic nude mice (21−23 g) were supplied by the Laboratory Animal Center of Sichuan University (Sichuan, China), and maintained in a light-controlled room kept at a temperature of 25 ± 2 °C and a relative humidity of 55 ± 5% with free access to standard food and water. The animals were fasted for at least 24 h prior to experiment but given water freely. Subcutaneous tumors were induced in either the left or right forelimb oxter of nude mice after inoculation of 4×10^6 A431 cells. The tumors were allowed to grow to ~30 mm^3 before experimentation.

Pharmacokinetics and Biodistribution. For pharmacokinetic studies, SD rats were randomly assigned to three groups, and each group received intravenous injection of Taxol, GH/PTX and GHC/PTX micellar formulations at a dose of 5 mg/kg, respectively. After administration, approximate 0.25 mL of blood was collected by heparinized tube from the orbital venous plexus at 15, 30 min, 1, 2, 4, 7, 12, and 24 h. Plasma samples were harvested by immediately centrifugation at 3000 r/min for 5 min and stored at −20 °C.

To assess the tissue distribution of PTX formulations, the A431 tumor-bearing mice were intravenously injected *via* tail vein with Taxol, GH/PTX and GHC/PTX, at a dose of 5 mg/kg. Mice were sacrificed at 30 min, 2 h, and 8 h after drug administration, and the heart, liver, spleen, lung, kidney, stomach, intestine and tumor were collected. Tissue samples were rinsed in saline, blotted with paper towel, weighed and stored at −20 °C.

Plasma concentrations of PTX were determined by HPLC. Briefly, 200 μL of plasma and 10 μL of internal standard (diazepam, 5 μg/mL) were extracted twice with 0.5 mL of MTBE. The organic layer was separated by centrifugation at 5000 r/min for 10 min and collected into a clean tube. The drug residue was obtained by evaporation and reconstituted in 100 μL mobile phase, and 50 μL of the supernatant was injected into the HPLC system. The flow rate was 1.0 mL/min, and the mobile phase consisted of methanol/water (70/30 v/v). The detection of PTX was performed by UV absorption at 227 nm. To determine tissue distribution of PTX, tissue samples were homogenized in saline. The homogenate (0.5 mL) was mixed with 50 μL of diazepam and extracted trice with 0.5 mL of MTBE. The drug residues were obtained and measured as described above.

***In Vivo* Optical Imaging.** A431 tumor-bearing mice were randomly assigned to two groups, and intravenously injected *via* tail vein with 200 μL of FITC-loaded MMPU nanomicelles (GH/FITC and GHC/FITC). The real-time images of the anesthetic mice were obtained by a macroimaging system LT-9 equipped with illumatool dual light system LT-99D2 (Lightools Research, Encinitas, CA, USA).

***In Vivo* Antitumor Activity.** To evaluate the antitumor effect of the MMPU nanosystems, Taxol at 6.6 mg/kg, GH/PTX at 3.5 mg/kg, GHC/PTX at 4.1 mg/kg, and PBS as a control group were intravenously injected through the tail vein once every 3 days for 18 days. Targeted (GHC) and nontargeted (GH) empty carriers without drug loading were also administrated at the same micellar dose and schedule as the PTX formulations. The length and width of the tumors were measured, and the tumor volume was calculated using the following formula: (width^2 × length)/2. The body weight and survival rate of each group were recorded for 20 days. After 20 day postinjection, mice were sacrificed, and the tumors were separated, weighed, and sectioned for histological evaluation with hematoxylin and eosin (H&E) staining.

Statistical Analysis. Data are expressed as means ± standard deviations (SD). The significance of difference was analyzed by one or two-way analysis of variance (ANOVA) using the Statistical Package for the Social Sciences (SPSS, version 19) software. Differences with $P < 0.05$ were considered statistically significant.

Conflict of Interest: The authors declare no competing financial interest.

Acknowledgment. The authors thank Prof. Zhirong Zhang and Xun Sun (Sichuan University, China) for the use of the macroimaging system, and Prof. Shaobing Zhou (Southwest Jiaotong University, China) for his help in size and zeta potential measurements. This work was supported by the National Natural Science Foundation of China (Grants 51073104, 51121001 and 51173118).

Supporting Information Available: Additional figures as described in the text: additional experimental details. This material is available free of charge *via* the Internet at http://pubs.acs.org.

REFERENCES AND NOTES

1. Farokhzad, O. C.; Langer, R. Impact of Nanotechnology on Drug Delivery. *ACS Nano* **2009**, *3*, 16–20.
2. Peer, D.; Karp, J. M.; Hong, S.; Farokhzad, O. C.; Margalit, R.; Langer, R. Nanocarriers As an Emerging Platform for Cancer Therapy. *Nat. Nanotechnol.* **2007**, *2*, 751–760.
3. Adair, J. H.; Parette, M. P.; Altnoglu, E. I.; Kester, M. Nanoparticulate Alternatives for Drug Delivery. *ACS Nano* **2010**, *4*, 4967–4970.
4. Wagner, V.; Dullaart, A.; Bock, A.; Zweck, A. The Emerging Nanomedicine Landscape. *Nat. Biotechnol.* **2006**, *24*, 1211–1217.
5. Davis, M. E.; Chen, Z. G.; Shin, D. M. Nanoparticle Therapeutics: An Emerging Treatment Modality for Cancer. *Nat. Rev. Drug. Discov.* **2008**, *7*, 771–782.
6. Cheng, Z.; Al Zaki, A.; Hui, J. Z.; Muzykantov, V. R.; Tsourkas, A. Multifunctional Nanoparticles: Cost *versus* Benefit of Adding Targeting and Imaging Capabilities. *Science* **2012**, *338*, 903–910.
7. Yan, Y.; Such, G. K.; Johnston, A. P. R.; Best, J. P.; Caruso, F. Engineering Particles for Therapeutic Delivery: Prospects and Challenges. *ACS Nano* **2012**, *6*, 3663–3669.
8. Gu, F.; Zhang, L.; Teply, B. A.; Mann, N.; Wang, A.; Radovic-Moreno, A. F.; Langer, R.; Farokhzad, O. C. Precise Engineering of Targeted Nanoparticles by Using Self-Assembled

Biointegrated Block Copolymers. *Proc. Natl. Acad. Sci. U.S.A.* **2008**, *105*, 2586–2591.
9. Torchilin, V. P. Multifunctional and Stimuli-sensitive Pharmaceutical Nanocarriers. *Eur. J. Pharm. Biopharm.* **2009**, *71*, 431–444.
10. Torchilin, V. P. Multifunctional Nanocarriers. *Adv. Drug Delivery Rev.* **2006**, *58*, 1532–1555.
11. Allen, T. M.; Cullis, P. R. Drug Delivery Systems: Entering the Mainstream. *Science* **2004**, *303*, 1818–1822.
12. Shi, J.; Votruba, A. R.; Farokhzad, O. C.; Langer, R. Nanotechnology in Drug Delivery and Tissue Engineering: From Discovery to Applications. *Nano Lett.* **2010**, *10*, 3223–3230.
13. Arias, J. L.; Reddy, L. H.; Othman, M.; Gillet, B.; Desmaele, D.; Zouhiri, F.; Dosio, F.; Gref, R.; Couvreur, P. Squalene-Based Nanocomposites: A New Platform for the Design of Multifunctional Pharmaceutical Theragnostics. *ACS Nano* **2011**, *5*, 1513–1521.
14. Wang, W.; Cheng, D.; Gong, F.; Miao, X.; Shuai, X. Design of Multifunctional Micelle for Tumor-Targeted Intracellular Drug Release and Fluorescent Imaging. *Adv. Mater.* **2012**, *24*, 115–120.
15. Dai, J.; Lin, S.; Cheng, D.; Zou, S.; Shuai, X. Interlayer-Crosslinked Micelle with Partially Hydrated Core Showing Reduction and pH Dual Sensitivity for Pinpointed Intracellular Drug Release. *Angew. Chem., Int. Ed.* **2011**, *50*, 9404–9408.
16. Quan, C.; Chen, J.; Wang, H.; Li, C.; Chang, C.; Zhang, X.; Zhuo, R. Core−Shell Nanosized Assemblies Mediated by the $\alpha-\beta$ Cyclodextrin Dimer with a Tumor-Triggered Targeting Property. *ACS Nano* **2010**, *4*, 4211–4219.
17. Lee, J. B.; Roh, Y. H.; Um, S. H.; Funabashi, H.; Cheng, W.; Cha, J. J.; Kiatwuthinon, P.; Muller, D. A.; Luo, D. Multifunctional Nanoarchitectures from DNA-Based ABC Monomers. *Nat. Nanotechnol.* **2009**, *4*, 430–436.
18. Li, Y.; Xiao, W.; Xiao, K.; Berti, L.; Luo, J.; Tseng, H. P.; Fung, G.; Lam, K. S. Well-Defined, Reversible Boronate Crosslinked Nanocarriers for Targeted Drug Delivery in Response to Acidic pH Values and *cis*-Diols. *Angew. Chem., Int. Ed.* **2012**, *51*, 2864–2869.
19. Yang, X.; Grailer, J. J.; Rowland, I. J.; Javadi, A.; Hurley, S. A.; Matson, V. Z.; Steeber, D. A.; Gong, S. Multifunctional Stable and pH-Responsive Polymer Vesicles Formed by Heterofunctional Triblock Copolymer for Targeted Anticancer Drug Delivery and Ultrasensitive MR Imaging. *ACS Nano* **2010**, *4*, 6805–6817.
20. Zhu, L.; Kate, P.; Torchilin, V. P. Matrix Metalloprotease 2-Responsive Multifunctional Liposomal Nanocarrier for Enhanced Tumor Targeting. *ACS Nano* **2012**, *6*, 3491–3498.
21. Xiao, W.; Chen, W.; Xu, X.; Li, C.; Zhang, J.; Zhuo, R.; Zhang, X. Design of a Cellular-Uptake-Shielding "Plug and Play" Template for Photo Controllable Drug Release. *Adv. Mater.* **2011**, *23*, 3526–3530.
22. Elsabahy, M.; Wazen, N.; Bayó-Puxan, N.; Deleavey, G.; Servant, M.; Damha, M. J.; Leroux, J. Delivery of Nucleic Acids through the Controlled Disassembly of Multifunctional Nanocomplexes. *Adv. Funct. Mater.* **2009**, *19*, 3862–3867.
23. Abeylath, S. C.; Ganta, S.; Iyer, A. K.; Amiji, M. Combinatorial-Designed Multifunctional Polymeric Nanosystems for Tumor-Targeted Therapeutic Delivery. *Acc. Chem. Res.* **2011**, *44*, 1009–1017.
24. Xiong, X.; Lavasanifar, A. Traceable Multifunctional Micellar Nanocarriers for Cancer-Targeted Co-Delivery of MDR-1 siRNA and Doxorubicin. *ACS Nano* **2011**, *5*, 5202–5213.
25. Yang, X.; Grailer, J. J.; Rowland, I. J.; Javadi, A.; Hurley, S. A.; Steeber, D. A.; Gong, S. Multifunctional SPIO/DOX-Loaded Wormlike Polymer Vesicles for Cancer Therapy and MR Imaging. *Biomaterials* **2010**, *31*, 9065–9073.
26. Lu, P.; Chen, Y.; Ou, T.; Chen, H.; Tsai, H.; Wen, C.; Lo, C.; Wey, S.; Lin, K.; Yen, T.; *et al*. Multifunctional Hollow Nanoparticles Based on Graft-Diblock Copolymers for Doxorubicin Delivery. *Biomaterials* **2011**, *32*, 2213–2221.
27. Xiao, Y.; Hong, H.; Javadi, A.; Engle, J. W.; Xu, W.; Yang, Y.; Zhang, Y.; Barnhart, T. E.; Cai, W.; Gong, S. Multifunctional Unimolecular Micelles for Cancer-Targeted Drug Delivery and Positron Emission Tomography Imaging. *Biomaterials* **2012**, *33*, 3071–3082.
28. Huang, C. K.; Lo, C. L.; Chen, H. H.; Hsiue, G. H. Multifunctional Micelles for Cancer Cell Targeting, Distribution Imaging, and Anticancer Drug Delivery. *Adv. Funct. Mater.* **2007**, *17*, 2291–2297.
29. Boretos, J. W.; Pierce, W. S. Segmented Polyurethane: A New Elastomer for Biomedical Applications. *Science* **1967**, *158*, 1481–1482.
30. Vermette, P.; Griesser, H. J.; Laroche, G.; Guidoin, R. *Biomedical Applications of Polyurethanes*, 6th ed.; Landes Bioscience: Austin, TX, 2001.
31. Ding, M.; Li, J.; Tan, H.; Fu, Q. Self-Assembly of Biodegradable Polyurethanes for Controlled Delivery Applications. *Soft Matter* **2012**, *8*, 5414–5428.
32. Ding, M.; He, X.; Wang, Z.; Li, J.; Tan, H.; Deng, H.; Fu, Q.; Gu, Q. Cellular Uptake of Polyurethane Nanocarriers Mediated by Gemini Quaternary Ammonium. *Biomaterials* **2011**, *32*, 9515–9524.
33. Ding, M.; Li, J.; Fu, X.; Zhou, J.; Tan, H.; Gu, Q.; Fu, Q. Synthesis, Degradation, and Cytotoxicity of Multiblock Poly(ε-caprolactone urethane)s Containing Gemini Quaternary Ammonium Cationic Groups. *Biomacromolecules* **2009**, *10*, 2857–2865.
34. Ding, M.; Zhou, L.; Fu, X.; Tan, H.; Li, J.; Fu, Q. Biodegradable Gemini Multiblock Poly(ε-caprolactone urethane)s Toward Controllable Micellization. *Soft Matter* **2010**, *6*, 2087–2092.
35. Ding, M.; He, X.; Zhou, L.; Li, J.; Tan, H.; Fu, X.; Fu, Q. Nontoxic Gemini Cationic Biodegradable Polyurethane Drug Carriers: Synthesis, Self-Assembly and *in Vitro* Cytotoxicity. *J. Controlled Release* **2011**, *152*, e87–e89.
36. Ding, M.; Qian, Z.; Wang, J.; Li, J.; Tan, H.; Gu, Q.; Fu, Q. Effect of PEG Content on the Properties of Biodegradable Amphiphilic Multiblock Poly(ε-caprolactone urethane)s. *Polym. Chem.* **2011**, *2*, 885–891.
37. Zhou, L.; Liang, D.; He, X.; Li, J.; Tan, H.; Li, J.; Fu, Q.; Gu, Q. The Degradation and Biocompatibility of pH-Sensitive Biodegradable Polyurethanes for Intracellular Multifunctional Antitumor Drug Delivery. *Biomaterials* **2012**, *33*, 2734–2745.
38. Zhou, L.; Yu, L.; Ding, M.; Li, J.; Tan, H.; Wang, Z.; Fu, Q. Synthesis and Characterization of pH-Sensitive Biodegradable Polyurethane for Potential Drug Delivery Applications. *Macromolecules* **2011**, *44*, 857–864.
39. Yang, X.; Du, J.; Dou, S.; Mao, C.; Long, H.; Wang, J. Sheddable Ternary Nanoparticles for Tumor Acidity-Targeted siRNA Delivery. *ACS Nano* **2011**, *6*, 771–781.
40. Zhu, M.; Nie, G.; Meng, H.; Xia, T.; Nel, A.; Zhao, Y. Physicochemical Properties Determine Nanomaterial Cellular Uptake, Transport, and Fate. *Acc. Chem. Res.* DOI: 10.1021/ar300031y.
41. Ulbrich, K.; Subr, V. Polymeric Anticancer Drugs with pH-Controlled Activation. *Adv. Drug Delivery Rev.* **2004**, *56*, 1023–1050.
42. Patra, C. R.; Bhattacharya, R.; Wang, E.; Katarya, A.; Lau, J. S.; Dutta, S.; Muders, M.; Wang, S.; Buhrow, S. A.; Safgren, S. L.; *et al*. Targeted Delivery of Gemcitabine to Pancreatic Adenocarcinoma Using Cetuximab as a Targeting Agent. *Cancer Res.* **2008**, *68*, 1970–1978.
43. Mamot, C.; Drummond, D. C.; Noble, C. O.; Kallab, V.; Guo, Z.; Hong, K.; Kirpotin, D. B.; Park, J. W. Epidermal Growth Factor Receptor-Targeted Immunoliposomes Significantly Enhance the Efficacy of Multiple Anticancer Drugs *in Vivo*. *Cancer Res.* **2005**, *65*, 11631–11638.
44. Kirpotin, D. B.; Drummond, D. C.; Shao, Y.; Shalaby, M. R.; Hong, K.; Nielsen, U. B.; Marks, J. D.; Benz, C. C.; Park, J. W. Antibody Targeting of Long-Circulating Lipidic Nanoparticles Does Not Increase Tumor Localization but Does Increase Internalization in Animal Models. *Cancer Res.* **2006**, *66*, 6732–6740.
45. Moghimi, S. M.; Hunter, A. C.; Murray, J. C. Long-Circulating and Target-Specific Nanoparticles: Theory to Practice. *Pharmacol. Rev.* **2001**, *53*, 283–318.

46. Sugahara, K. N.; Teesalu, T.; Karmali, P. P.; Kotamraju, V. R.; Agemy, L.; Girard, O. M.; Hanahan, D.; Mattrey, R. F.; Ruoslahti, E. Tissue-Penetrating Delivery of Compounds and Nanoparticles into Tumors. *Cancer Cell* **2009**, *16*, 510–520.
47. Ke, X.; Zhao, B.; Zhao, X.; Wang, Y.; Huang, Y.; Chen, X.; Zhao, B.; Zhao, S.; Zhang, X.; Zhang, Q. The Therapeutic Efficacy of Conjugated Linoleic Acid-Paclitaxel on Glioma in the Rat. *Biomaterials* **2010**, *31*, 5855–5864.
48. Zhang, C.; Qu, G.; Sun, Y.; Wu, X.; Yao, Z.; Guo, Q.; Ding, Q.; Yuan, S.; Shen, Z.; Ping, Q.; *et al*. Pharmacokinetics, Biodistribution, Efficacy and Safety of *N*-Octyl-*O*-Sulfate Chitosan Micelles Loaded with Paclitaxel. *Biomaterials* **2008**, *29*, 1233–1241.
49. Li, Y.; Xiao, K.; Luo, J.; Xiao, W.; Lee, J. S.; Gonik, A. M.; Kato, J.; Dong, T. A.; Lam, K. S. Well-Defined, Reversible Disulfide Cross-Linked Micelles for On-Demand Paclitaxel Delivery. *Biomaterials* **2011**, *32*, 6633–6645.
50. Gullotti, E.; Yeo, Y. Extracellularly Activated Nanocarriers: A New Paradigm of Tumor Targeted Drug Delivery. *Mol. Pharm.* **2009**, *6*, 1041–1051.
51. Baselga, J. The EGFR as a Target for Anticancer Therapy-Focus on Cetuximab. *Eur. J. Cancer* **2001**, *37*, 16–22.
52. Cho, Y. W.; Lee, J.; Lee, S. C.; Huh, K. M.; Park, K. Hydrotropic Agents for Study of *in Vitro* Paclitaxel Release from Polymeric Micelles. *J. Controlled Release* **2004**, *97*, 249–257.
53. Talelli, M.; Rijcken, C. J. F.; Oliveira, S.; van der Meel, R.; van Bergen En Henegouwen, P. M. P.; Lammers, T.; van Nostrum, C. F.; Storm, G.; Hennink, W. E. Nanobody-Shell Functionalized Thermosensitive Core-Crosslinked Polymeric Micelles for Active Drug Targeting. *J. Controlled Release* **2011**, *151*, 183–192.